Studies of emittance growth and halo particle production in intense charged particle beams using the Paul Trap Simulator Experimenta)

Erik P. Gilson, Ronald C. Davidson, Mikhail Dorf, Philip C. Efthimion, Richard Majeski, Moses Chung, Michael S. Gutierrez, and Aaron N. Kabcenell

Citation: Physics of Plasmas **17**, 056707 (2010); doi: 10.1063/1.3354109
View online: http://dx.doi.org/10.1063/1.3354109
View Table of Contents: http://scitation.aip.org/content/aip/journal/pop/17/5?ver=pdfcov
Published by the AIP Publishing

Studies of emittance growth and halo particle production in intense charged particle beams using the Paul Trap Simulator Experiment[a)]

Erik P. Gilson,[1,b)] Ronald C. Davidson,[1] Mikhail Dorf,[1] Philip C. Efthimion,[1] Richard Majeski,[1] Moses Chung,[2] Michael S. Gutierrez,[3] and Aaron N. Kabcenell[4]
[1]*Plasma Physics Laboratory, Princeton University, Princeton, New Jersey 08543, USA*
[2]*Accelerator Physics Center, Fermi National Accelerator Laboratory, Batavia, Illinois 60510, USA*
[3]*University of California Los Angeles, Los Angeles, California 90095, USA*
[4]*Weston High School, Weston, Connecticut 06883, USA*

(Received 1 December 2009; accepted 12 February 2010; published online 12 April 2010)

The Paul Trap Simulator Experiment (PTSX) is a compact laboratory experiment that places the physicist in the frame-of-reference of a long, charged-particle bunch coasting through a kilometers-long magnetic alternating-gradient (AG) transport system. The transverse dynamics of particles in both systems are described by the same set of equations, including nonlinear space-charge effects. The time-dependent voltages applied to the PTSX quadrupole electrodes in the laboratory frame are equivalent to the spatially periodic magnetic fields applied in the AG system. The transverse emittance of the charge bunch, which is a measure of the area in the transverse phase space that the beam distribution occupies, is an important metric of beam quality. Maintaining low emittance is an important goal when defining AG system tolerances and when designing AG systems to perform beam manipulations such as transverse beam compression. Results are reviewed from experiments in which white noise and colored noise of various amplitudes and durations have been applied to the PTSX electrodes. This noise is observed to drive continuous emittance growth and increase in root-mean-square beam radius over hundreds of lattice periods. Additional results are reviewed from experiments that determine the conditions necessary to adiabatically reduce the charge bunch's transverse size and simultaneously maintain high beam quality. During adiabatic transitions, there is no change in the transverse emittance. The transverse compression can be achieved either by a gradual change in the PTSX voltage waveform amplitude or frequency. Results are presented from experiments in which low emittance is achieved by using focusing-off-defocusing-off waveforms. © *2010 American Institute of Physics*.
[doi:10.1063/1.3354109]

I. INTRODUCTION

Intense beam propagation[1–6] is an active area of research and is at the center of various scientific studies, including heavy ion fusion, ion-beam-driven high energy density physics, spallation neutron sources, high energy physics, nonlinear dynamics, and nuclear waste transmutation.[7] The Paul Trap Simulator Experiment (PTSX) simulates, in a compact cylindrical Paul trap,[8] intense beams that propagate for equivalent distances in alternating-gradient (AG) focusing systems of over 10 km.[9] This allows the study of important scientific topics such as: the conditions for quiescent beam propagation, collective mode excitation, beam-mismatch effects, emittance growth, generation and dynamics of halo particles, and distribution function effects.[10–13] At the high beam intensities envisioned in present and next-generation facilities, a fundamental understanding of the influence of collective processes and self-field effects on beam transport and stability properties must be developed. In this paper, attention is given to studies to understand emittance growth and halo particle production.

In intense charged particle beams, the space-charge effects are sufficiently strong that they affect the dynamics of the beam propagation. The strength of the transverse space-charge force is characterized by the plasma frequency $\omega_p(r)=[n_b e_b^2/m_b\epsilon_0]^{1/2}$, whereas the transverse confining force is characterized by the average transverse focusing frequency ω_q of the transverse oscillations of a particle in an AG system.[1] Here, ϵ_0 is the permittivity of free space, $n_b(r)$ is the radial density profile, and e_b and m_b are the ion charge and mass, respectively. The normalized intensity parameter $\hat{s}=\omega_p^2(0)/2\omega_q^2$ describes whether the beam is emittance dominated ($\hat{s}\ll 1$) or space-charge dominated ($\hat{s}\to 1$). Emittance is the effective area that the beam particles occupy in two-dimensional (2D) position/velocity phase space and is proportional to the root-mean-square radius of the beam R_b and the average transverse velocity of the particles as characterized by the temperature $\sqrt{kT/m}$. For example, Fermilab's Tevatron injector typically operates at $\hat{s}\sim 0.15$, and the Spallation Neutron Source is expected to operate at $\hat{s}\sim 0.2$. The PTSX device presently operates in the range $0<\hat{s}\lesssim 0.5$.[9]

Using a linear Paul trap confining a one-component plasma to study nonlinear beam dynamics was proposed by Davidson *et al.*[14] and by Okamoto and Tanaka.[15–17] The $e_b\boldsymbol{E}_\perp^{\rm ext}$ forces that the PTSX electrodes exert on the trapped

[a)]Paper CI2 3, Bull. Am. Phys. Soc. **54**, 54 (2009).
[b)]Invited speaker. Electronic mail: egilson@pppl.gov.

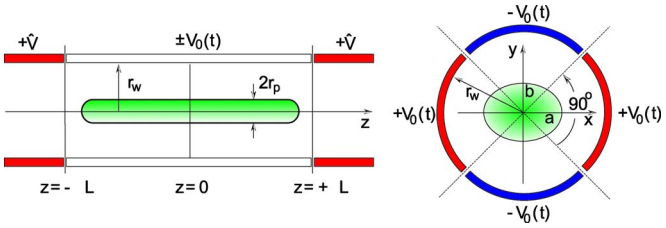

FIG. 1. (Color online) The PTSX device consists of three cylindrical electrodes with radius $r_w=0.1$ m, each divided into four 90° sectors. An oscillating voltage $\pm V_0(t)$ confines the plasma in the transverse plane to a radius r_p. Static voltages $+\hat{V}$ on the end electrodes confine the ions axially within a length $2L=2$ m.

plasma particles are analogous to the $e_b \boldsymbol{v}_z \times \boldsymbol{B}_\perp^{\text{ext}}$ forces that the AG system exert on the beam particles in the beam frame provided that long, coasting beams that are thin relative to the AG system magnet spacing are considered. Specifically, the amplitude and frequency of the voltage waveform applied to the PTSX electrodes correspond to the quadrupole magnet strength and lattice spacing in the AG system. In addition to the equivalence of the applied forces, the self-field forces in both systems can be described by scalar potentials that obey Poisson's equation. In Ref. 14, it was shown that the self-consistent transverse Hamiltonians and the resulting Vlasov equations for the AG system and the PTSX system are equivalent, neglecting end effects. Thus, the very good confinement properties of ions in PTSX and the arbitrary form of the voltage waveform applied to the confining electrodes make PTSX a compact, flexible laboratory facility in which to simulate intense beam propagation through AG systems.

In this paper, a description of the PTSX device is given (Sec. II), and relevant background information is summarized (Sec. III). Three different experiments are discussed, each in the context of emittance growth and halo particle production. The effects of noise on emittance growth and halo particle production are presented in Sec. IV.[18,19] Experimental results that examine the effects of varying both the amplitude and frequency of the applied voltage waveform are presented (Sec. V).[20,21] Finally, the reduction in the initial emittance by using focusing-off-defocusing-off (FODO) waveforms instead of sinusoidal waveforms is shown in Sec. VI.

II. EXPERIMENTAL APPARATUS

The PTSX device has been described elsewhere[22–26] and only a brief description is presented here. The PTSX device (see Fig. 1) is a linear Paul trap and consists of three colinear cylinders with radius $r_w=0.1$ m, each divided into four 90° azimuthal sectors, in a vacuum of 1×10^{-9} Torr. The pure cesium-ion plasma is confined radially in the central 2 m long cylinder by oscillating voltages (typically 150 V at 60 kHz) applied as shown in Fig. 1. The outer two cylinders are each 0.4 m long and the voltage on these electrodes is held fixed at 50 V in order to confine the plasma axially. To inject or dump the ions, the voltage on one or the other set of outer electrodes is switched to the same oscillating voltage that is applied to the central cylinder. The time duration of injection (t_i), trapping (t_t), and dumping (t_d) may be varied independently with typical values being $t_i=1.7$ ms, $t_t\leq300$ ms, and $t_d\geq10$ ms.

The cesium ion source consists of an aluminosilicate emitter surrounded by a Pierce electrode, followed by an acceleration grid and a deceleration grid to extract the desired ion current and adjust the final ion kinetic energy. Extraction voltages of less than 10 V are required to extract sufficient cesium current to fill the trap to a normalized intensity parameter of $\hat{s}=0.5$. Values of the normalized intensity parameter closer to unity have not been achieved in PTSX because the ion source is not ideal and, further, the source injects plasmas that are not perfectly matched to the time-dependent oscillating voltage waveform. These effects cause the trapped plasma to have a large enough effective transverse temperature that a significant portion of the confining force must be utilized to counteract the thermal pressure when it could otherwise be used to balance the space-charge of a denser plasma.

At the opposite end of PTSX from the ion source, there is a 5-mm-diameter circular copper collector. The collector is moveable in the transverse direction in order to measure the z-integrated radial charge profile. This collector moves along a null of the time-dependent applied voltage waveform in order to minimally disturb the electrostatic potential structure. Due to the relatively low injected axial velocity of ions in PTSX, it takes several milliseconds, or several hundred lattice periods, for the trapped plasma to be completely collected. The measured charge profile is therefore necessarily time averaged.

III. BACKGROUND

The details of the analogy between AG systems and linear Paul traps such as PTSX are presented in Ref. 14. Here, we discuss the average transverse oscillation frequency ω_q, the force-balance equation that determines the root-mean-square beam radius, and the transverse emittance of the plasma. The transverse motion of particles in either an AG system or in a Paul trap consists of rapid micromotion arising from the periodic focusing and defocusing forces, superimposed on a guiding-center oscillation. The smooth-focusing approximation can be invoked to average over the rapid oscillations when the timescales of the two motions are well separated. The oscillation frequency of the average transverse motion ω_q, neglecting space-charge effects, is then given by a simple analytical formula.[1,9]

In the PTSX system, transverse confinement can be described in terms of a ponderomotive force acting on the particles. For the circular PTSX electrodes, the applied electric potential near the axis at $r=0$ is[14]

$$e_b\phi_{\text{ap}}(x,y,t)=\tfrac{1}{2}\kappa_q(t)(x^2-y^2), \tag{1}$$

where $\kappa_q(t)=8e_bV_0(t)/m_b\pi r_w^2$. The voltage applied to the electrodes has the form $\pm V_0(t)=\pm V_{0\,\max}g(t)$, and $g(t)$ is a periodic function with unit amplitude and frequency f. For $r/r_w\ll1$, the resulting ponderomotive force is proportional to the displacement from the axis, and the frequency of the

transverse oscillations is given in the smooth-focusing approximation by[1,9,22,23]

$$\omega_q = \frac{8e_b V_{0\,\max}}{m_b r_w^2 \pi f}\xi, \tag{2}$$

where $m_b = 133$ amu for Cs^+ ions in PTSX. The factor ξ depends on the shape of the voltage waveform $g(t)$: $\xi = 1/2\sqrt{2}\pi$ for a sinusoidal waveform, and $\xi = \eta\sqrt{3-2\eta}/(4\sqrt{3})$ for a periodic step-function waveform with fill-factor η (the so-called FODO lattice).

Under quasisteady-state conditions, for a thermal equilibrium distribution of particles, the average density profile $n_b(r)$ is given by[1,2]

$$n_b(r) = n_b(r=0)\exp\left[-\frac{m_b\omega_q^2 r^2 + 2e_b\phi^s(r)}{2kT}\right]. \tag{3}$$

Here, k is Boltzmann's constant, T=const. is the transverse temperature, and the space-charge potential $\phi^s(r)$ is determined self-consistently from Poisson's equation $r^{-1}\partial_r(r\partial_r\phi^s) = -n_b(r)e_b/\epsilon_0$. For $kT \to 0$, the numerator in the exponential must also approach zero in order for the density to remain finite and this implies a nearly uniform density plasma. In the case of low space-charge density, the electrostatic potential term in the exponential can be neglected and the radial density profile is nearly Gaussian.

Integration of Eq. (3) over the radial distribution gives the global radial force-balance equation[1]

$$m_b\omega_q^2 R_b^2 = 2kT + \frac{N_b e_b^2}{4\pi\epsilon_0}, \tag{4}$$

where $N_b = \int_0^{r_w} n_b(r) 2\pi r dr$ is the line density, and $R_b^2 = (1/N_b)\int_0^{r_w} n_b(r) 2\pi r^3 dr$ is the mean-square radius of the plasma column. In PTSX experiments, R_b^2 and N_b are calculated from the measured plasma density profiles; kT is the only parameter not known *a priori* and is inferred from Eq. (4). The effective emittance ϵ is a measure of the area in transverse phase space that the beam particle distribution occupies and is defined here to be

$$\epsilon = 2R_b\left(\omega_q^2 R_b^2 - \frac{N_b e_b^2}{4\pi\epsilon_0 m_b}\right)^{1/2}. \tag{5}$$

For the data presented here, the voltage applied to the 0.6 in. diameter emitting surface of the cesium source was 3 V, while the voltage on the acceleration grid was 1.6 V. The deceleration grid was held fixed at 0 V. The plasmas were injected for 1.7 ms, trapped for up to 100 ms, and then dumped. The radial charge profile, which is proportional to $n_b(r)$, is then measured by averaging the signal at each radial position over several hundred shots of PTSX. The area of the collector aperture and an estimate of the plasma length L_p (Ref. 27) are then used to calculate $n_b(r)$. Typical peak densities are less than 5×10^5 cm^{-3}.

To make use of Eq. (4) in order to measure the effective transverse temperature of the plasma, N_b and R_b are obtained from the experimental data by integrating the appropriate moments of the measured radial density profile $n_b(r)$ of the trapped plasma. The parameter $\hat{s} = \omega_p^2(0)/2\omega_q^2$ is extracted from the measured density profile $n_b(r)$ by using the on-axis value $n_b(0)$. The effective emittance is then computed using Eq. (5).

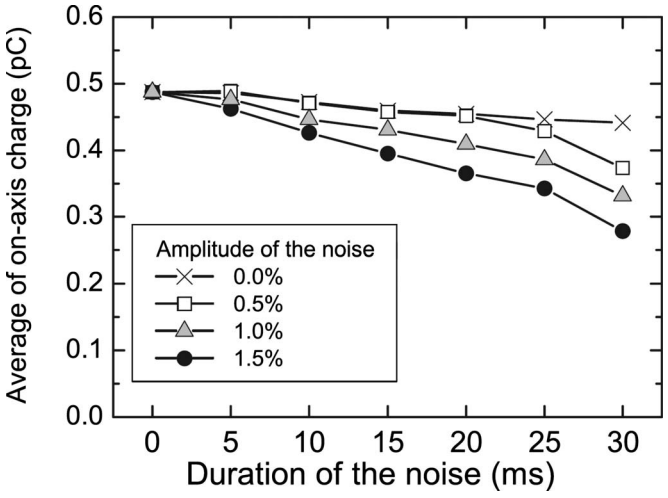

FIG. 2. Reprinted from Refs. 18 and 19. The on-axis signal vs time averaged over 20 error samples for different white noise amplitudes.

IV. NOISE-INDUCED DEGRADATION OF BEAM QUALITY

The presence of undesired random noise due to machine imperfections and its influence on the long-time-scale beam dynamics is an important issue in accelerator design.[28,29] For example, machine imperfections such as quadrupole magnet and rf cavity alignment errors, quadrupole focusing gradient errors, and rf field amplitude and phase errors can all contribute to a degradation of the beam quality.[30] Therefore, it is important to understand the effects of random noise on long-distance beam propagation, including the effects of moderate space charge. Recent PTSX experiments[18,19] have demonstrated the effects on the emittance of a beam due to white noise, and the combined effects of colored noise together with mismatch oscillations. In this section, a brief review of these experiments is given.

The PTSX arbitrary function generator allows for multiple sets of noise lattice waveforms to be created and applied repeatedly to trapped plasmas. In these experiments, the amplitude of each half-period of a sinusoidal applied voltage waveform was varied by a random amount chosen according to a particular distribution. In the case of white noise, the amplitude of the n^{th} half-period was varied by an amount δ_n chosen from a uniform distribution such that $|\delta_n| \le \Delta_{\max}$, where $\Delta_{\max}$ is the maximum variation. Values of $\Delta_{\max}$ up to 1.5% were studied and these noisy lattice waveforms were applied for various plasma trapping times corresponding to up to 1800 lattice periods of equivalent beam propagation. In the case of colored noise, δ_n was chosen according to $\delta_{n+1} = \delta_n \exp(-T/2\tau_{ac}) + w_n\Delta_{\max}[1-\exp(-T/\tau_{ac})]^{1/2}$, where T is the lattice period, τ_{ac} is the autocorrelation time, and w_n is a Gaussian-distributed random number with unit variance.

Initial experiments using white noise confirmed that noisy lattice waveforms caused the root-mean-square radius R_b to grow with time and, therefore, the on-axis signal to

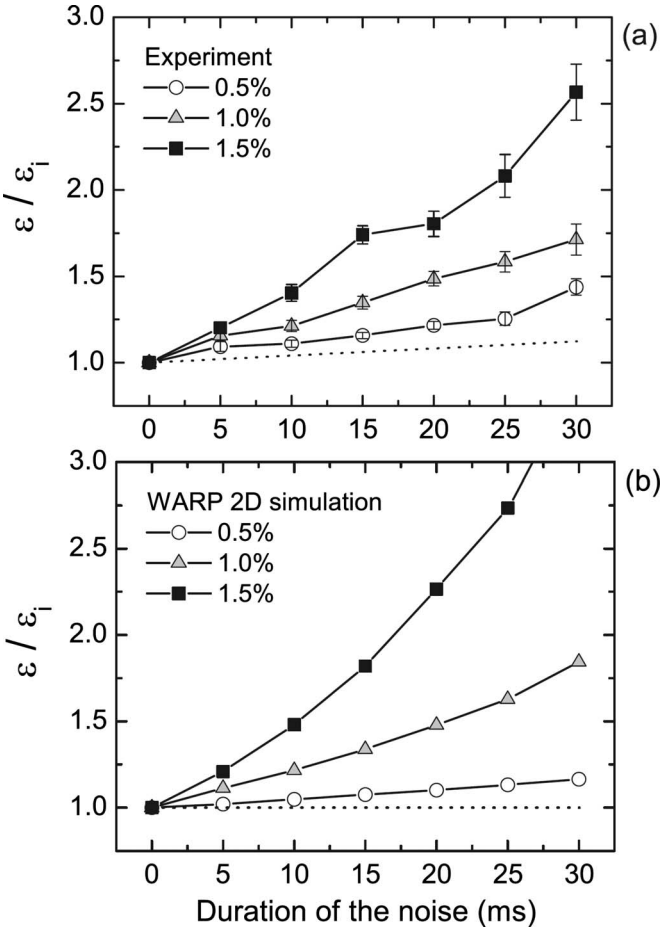

FIG. 3. Reprinted from Refs. 18 and 19. (a) The effective emittance vs time for several white noise amplitudes as computed from the measured transverse density profiles. (b) The effective emittance as computed from 2D Warp simulations using 20 error sets. The dotted lines represent the effective emittance growth in the absence of applied noise. In the experiment, there is residual effective emittance growth due to inherent noise.

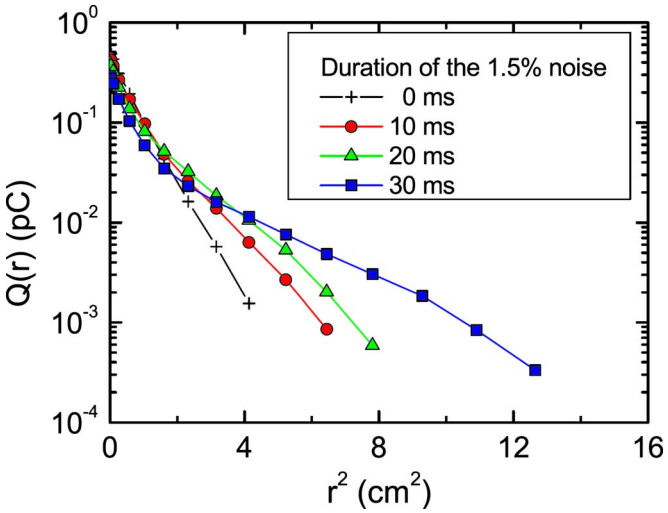

FIG. 4. (Color online) Reprinted from Refs. 18 and 19. Measured radial density profiles with different noise amplitudes and durations. The initial state is a Gaussian, but at later times develops a large halo population of tail particles.

decrease with time. For example, as shown in Fig. 2 (from Refs. 18 and 19), 1.5% amplitude noise applied for 1800 lattice periods caused a 40% decrease in on-axis signal on average. The variance in the on-axis signal measurements also increased with the duration of the noise, but the data did not conclusively show whether the rate of increase scaled as $t^{1/2}$ as in a random walk.

Both the experimental data and 2D Warp particle-in-cell simulations[31] showed that the root-mean-square beam radius R_b increased linearly with the duration of the applied noise. Since the emittance scales as R_b^2, it was expected that the emittance would grow linearly for small noise amplitudes and quadratically for larger noise amplitudes. Indeed, both the experimental results and 2D Warp simulation results show these dependencies on noise amplitude (Fig. 3, taken from Refs. 18 and 19).

Especially noteworthy is the distortion of the average transverse plasma density profile for the large noise amplitudes and durations seen in Fig. 4 (from Refs. 18 and 19). The data show a strong departure from a Gaussian profile, exhibiting depletion of particles at small radius, and a corresponding increase in the number of particles at large radius. This population of particles at large radius forms a sizeable population of halo particles.

Motivated by Bohn and Sideris,[28,32] experiments were also performed with colored noise.[33] Colored noise alone had a negligible effect on the plasma properties when the autocorrelation time was longer than approximately three lattice periods.[19] In this regime, the noise appears as a series of adiabatic amplitude changes that conserve emittance. Experiments in which a sudden mismatch is introduced by suddenly changing the voltage amplitude for one lattice period led to emittance growth and the creation of a population of halo particles. When noise with an autocorrelation time of five lattice periods was applied together with a sudden mismatch, the data in Fig. 5 (from Ref. 19) shows that the emittance growth and halo particle population were both seen to be larger.

V. EFFECTS OF COMPRESSION ON BEAM QUALITY

Transverse compression of a beam's radius is a common beam manipulation and it is important to understand the constraints that limit the ability to compress a beam without a loss in beam quality. The transverse compression should ideally be executed over as few lattice periods of the transport system as possible in order to keep the overall system length, and cost, minimized. However, transverse compression cannot be applied so rapidly as to drastically reduce the beam quality, excite collective-mode oscillations, or generate unwanted halo particles.[10–13,34] Recent PTSX experiments have explored adiabatic transverse bunch compression by increasing the average transverse focusing frequency ω_q.[21,20] Since $\omega_q \propto V_{0\,\max}/f$, either increases in $V_{0\,\max}$ or decreases in f will compress the plasma.

Figure 6 (from Refs. 20 and 35) shows the average transverse plasma density profile for the case of an instantaneous increase in $V_{0\,\max}$ of 90% and an adiabatic increase in $V_{0\,\max}$ of 90%. Here, the applied waveform frequency is 60 kHz, the initial voltage waveform amplitude is $V_{0\,\max}=150$ V, and

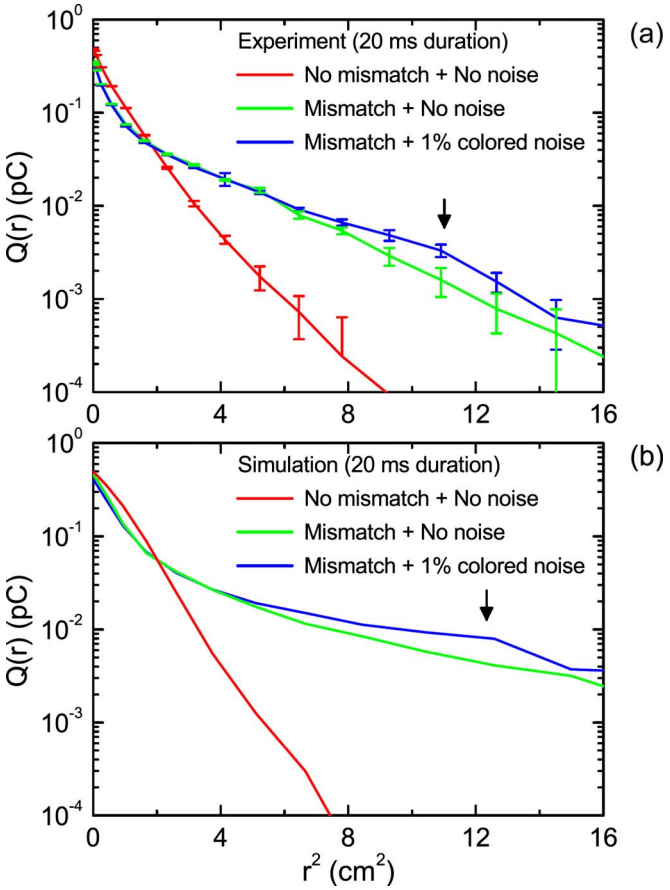

FIG. 5. (Color online) Reprinted from Ref. 19. (a) Radial density profiles for no perturbation, instantaneous mismatch only and both mismatch, and colored noise with $\tau_{ac}=5$. (b) 2D Warp simulations are in good agreement with the measured radial density profiles.

the adiabatic increase is applied over a number of lattice periods $N_t=40$ to ensure that the transition is truly adiabatic. Whereas the adiabatic change maintains the Gaussian profile, the instantaneous change causes particles to move from small radius and form a large population of halo particles at large radius. The adiabatic change causes an increase in the effective emittance of only 10%, whereas the instantaneous change increases the effective emittance by 140%.

In subsequent experiments, the number of lattice periods for the transition N_t was varied in order to determine the most rapid transition that was possible while still being adiabatic. The experimental results gave $N_{t\,\min}=4$, which is consistent with the notion that the condition for adiabaticity is that $N_t\omega_q/f>1$, where ω_b is the characteristic beam envelope oscillation frequency. Specifically, $N_t\omega_q/f\sim 7$ for these data. The measured transverse plasma density profiles for adiabatic transitions with $N_t=4$ and $N_t=20$ are almost identical, confirming that once the transition is sufficiently gradual to be considered adiabatic, there is no benefit to further increasing the transition time.

Generally, adiabatic changes conserve emittance and instantaneous changes conserve energy. This is demonstrated by the data in Fig. 7 (from Refs. 20 and 21), where both increases and decreases in $V_{0\,\max}$ are applied instantaneously and adiabatically. In the region $0.6<V_f/V_i<1.6$, the data are

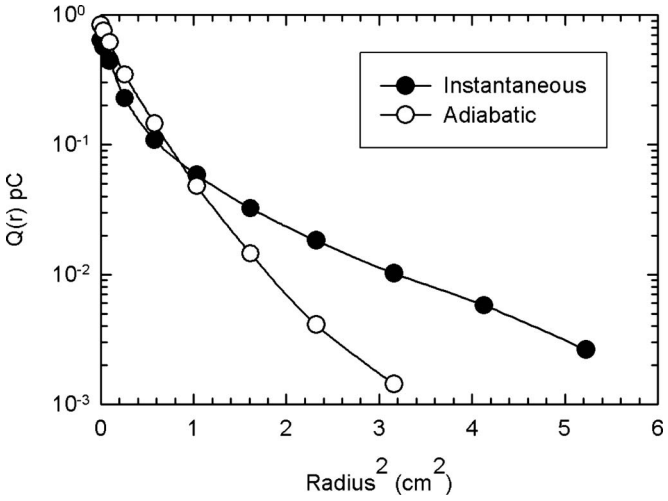

FIG. 6. Reprinted from Ref. 20, and from Ref. 35 with permission from Elsevier. The average transverse density profile remains approximately Gaussian when a 90% increase in $V_{0\,\max}$ is applied adiabatically. When applied instantaneously, particles are moved from the core to form a halo particle population at large radius.

in excellent agreement with a simple analytical estimate.[20] Note that for $V_f/V_i>1.6$ the single-particle vacuum phase advance is becoming too large, leading to unstable orbits and particle loss. For $V_f/V_i<0.6$, the average transverse focusing frequency ω_q is becoming too small and the plasma expansion causes particles to be lost to the wall.

These experiments were repeated using changes in the lattice frequency f instead of changes in $V_{0\,\max}$ and the results were similar. When the applied waveform frequency f was adiabatically decreased from 60 to 45 kHz at fixed amplitude $V_{0\,\max}=150$ V, the Gaussian transverse density profile was maintained.[21] As with the adiabatic voltage waveform amplitude changes, the change was sufficiently gradual to be considered adiabatic when $N_t=4$.[21] These experimental results confirmed that, when the smooth-focusing model is applicable, changes in either $V_{0\,\max}$ or f are effective in changing the average transverse focusing frequency ω_q.

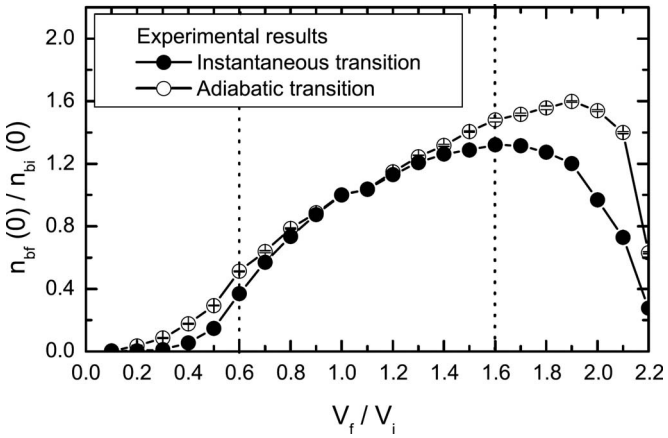

FIG. 7. Reprinted from Refs. 20 and 21. For transitions from an initial value $V_{0\,\max}=V_i$ to a final value V_f, adiabatic changes conserve emittance and the on-axis signal scales linearly with V_f/V_i over the range $0.6<V_f/V_i<1.6$. For instantaneous changes, where energy is conserved, the on-axis signal is less than in the adiabatic change case as V_f/V_i differs from unity.

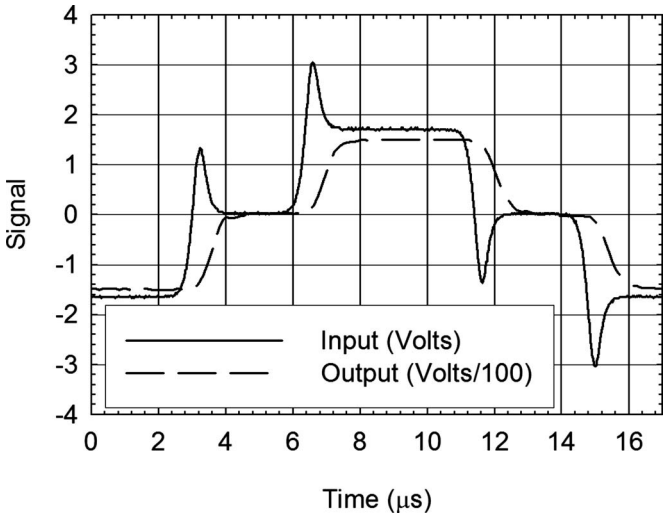

FIG. 8. An example of the input wave (solid line) required to produce a FODO waveform on the PTSX electrodes (dashed line). The input waveform must have an overshoot at each edge transition to compensate for the finite *RC* response time of the load. The input waves must also have a gradual rise and fall so that the output waveform has a gradual rise and fall to avoid Gibbs ringing.

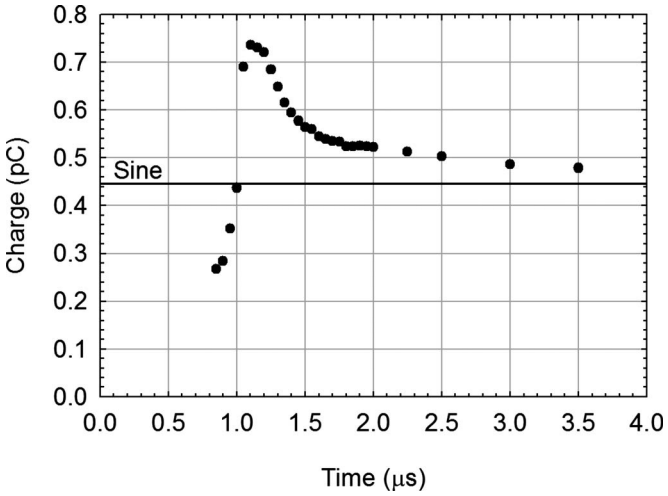

FIG. 9. The on-axis signal as a function of the characteristic FODO waveform rise time τ shows that for large τ, where the applied voltage waveform broadly resembles a sinusoid, the measurement is nearly the same is if a true sinusoid had been applied (solid line). As τ is reduced, the on-axis signal grows until τ becomes too short, Gibbs ringing in the applied waveform is seen, and and the on-axis signal drops sharply.

VI. FOCUSING-OFF-DEFOCUSING-OFF WAVEFORMS

A series of experiments were performed in which the voltage waveform applied to the PTSX electrodes was a periodic step function corresponding to a FODO magnetic lattice in an AG system. The FODO waveform represents a more accurate description of the periodic quadrupole magnetic field waveform than a sinusoidal waveform. It was expected that, for FODO waveform amplitudes, frequencies, and fill-factors such if that the average transverse focusing frequency is equal to that of a sinusoidal wave, the results of most experiments would be similar. However, it is observed that the use of FODO waveforms with the same average transverse focusing frequencies as a prescribed sinusoidal waveform produced plasmas that had higher total line charge N_b, greater normalized intensity $\hat{s}$, lower temperature kT, and reduced effective emittance ϵ.

There are several important considerations for applying FODO waveforms to the PTSX electrodes. First, the PTSX electrodes, together with the electrode amplifier circuits, have a finite *RC* response time. This results in distorted waveforms when ideal FODO waveforms are applied to the amplifier inputs. Second, the limited gain-bandwidth product of the amplifiers means that there will be Gibbs ringing even if the *RC* response time is short.

The finite *RC* response time can be overcome by overdriving the amplifiers at each transition in the FODO waveform. In practice, the amplitude of the overshoot is determined by trial and error for each FODO waveform amplitude. When the overshoot amplitude is optimized, the Gibbs ringing becomes apparent. To remove the unwanted oscillations, the sharp transitions of an ideal FODO waveform are replaced by smooth hyperbolic tangent transitions with variable time constant τ. The gradual transition of the transverse field from zero to its peak value better simulates the fringe fields of real quadrupole magnets used in actual AG systems. In most experiments, τ is set as small as possible. The data in Fig. 8 show the measured waveforms at the amplifier input and output. The input waveform consists of both an overshoot to compensate for the *RC* response time of the amplifier and load, and also a nonzero τ to avoid Gibbs ringing.

The requirement of a nonzero τ in order to have well-behaved voltage waveforms creates a lower limit on the duration of the voltage waveform step. This places constraints on the allowable values of the waveform frequency f and fill-factor η. At a given frequency, the fill-factor cannot be too small or else the voltage waveform does not have time to reach the flattop peak value. Similarly, at given fill-factor, the frequency cannot be too large.

The results in Fig. 9 demonstrate the effect on the on-axis trapped charge of varying the ramp-up time τ at a fixed voltage waveform amplitude $V_{0\,\max}=150$ V, frequency $f=60$ kHz, and fill-factor $\eta=0.6$. For large values of τ, the applied waveform broadly resembles a sinusoid and the value of the on-axis trapped charge is similar to that when a sinusoidal waveform is applied. However, as τ decreases, the value of the on-axis trapped charge rises. This rise continues until τ is small enough that the Gibbs ringing appears in the applied voltage waveform and the measured on-axis signal drops sharply. In subsequent experiments, τ is set to approximately 1.25 μs.

An experiment using 100 V, 60 kHz applied voltage waveforms is typical of the results observed when using FODO waveforms instead of sinusoidal waveforms (Fig. 10). When a sinusoidal waveform is used to inject, trap for 100 ms, and dump a plasma, the total line charge is measured to be 1.9×10^7 m^{-1}, the root-mean-square radius is 1.5 cm, and therefore the inferred temperature is 0.17 eV. The normalized intensity $\hat{s}$ is 0.16. Simply replacing the sinusoidal

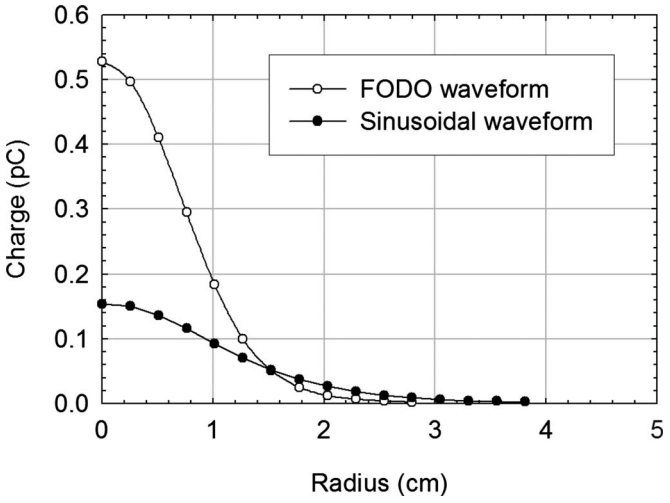

FIG. 10. The radial density profile for a 100 V 60 kHz sinusoidal applied waveform has R_b=1.5 cm, kT=0.17 eV, and $\hat{s}$=0.16 (black circles). The radial density profile for a 100 V, 60 kHz, η=0.577 FODO applied waveform has R_b=1.0 cm, kT=0.08 eV, and $\hat{s}$=0.45 (white circles). The effective emittance for the radial density profile corresponding to the FODO waveform is 45% of that for the case of the sinusoidal waveform.

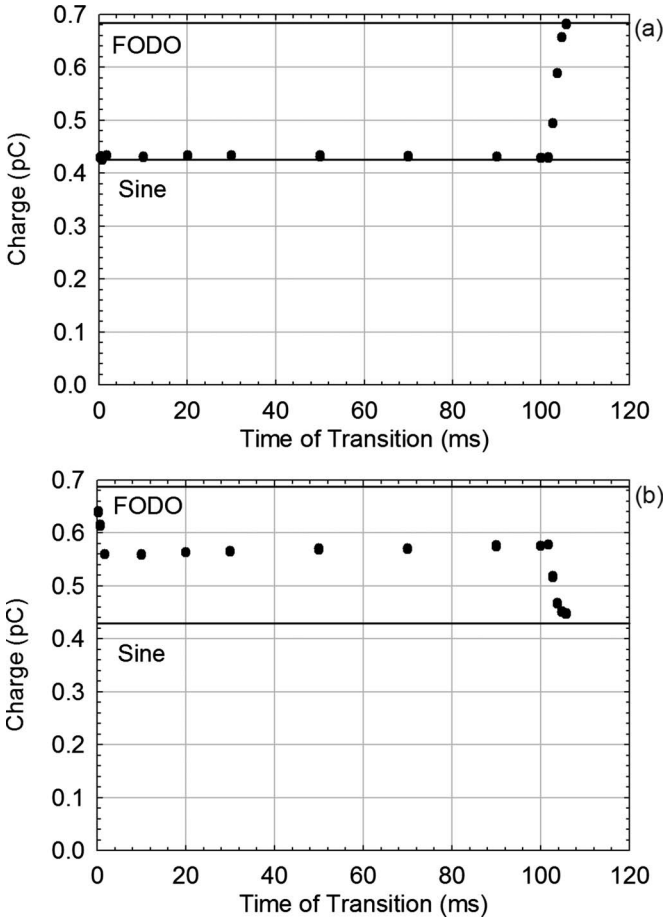

FIG. 11. (a) The on-axis signal measured after the applied waveform was switched from FODO to sinusoidal at a time t. For any time t before the dumping time at 101.7 ms, the change to a sinusoidal waveform causes the system to behave as though the sinusoidal waveform had been applied for all time. (b) The on-axis signal measured after the applied waveform was switched from sinusoidal to FODO at a time t. Although not as large a signal as when FODO waveforms are applied for all time, switching from sinusoidal to FODO during the trapping time increases the measured on-axis signal. During the trapping time, the ion source cannot affect the trapped plasma.

waveform with a FODO waveform with fill-factor η=0.577, the average transverse focusing frequency is unchanged, but the resulting plasma has different properties. In the case of the FODO applied voltage waveform, the total line charge is measured to be 3.0×10^7 m^{-1}, the root-mean-square radius is 1.0 cm, and therefore the inferred temperature is 0.08 eV. The normalized intensity is $\hat{s}$=0.45. The radii and temperatures of these two plasmas can be used to compute the relative effective emittance and it is found that the plasma trapped using the FODO waveform has an effective emittance that is 45% of the effective emittance for the case of the sinusoidal waveform.

It is known that the PTSX ion source creates plasmas that are initially mismatched to the lattice.[25] To test whether the differences in the line charges, root-mean-square radii, and inferred temperatures of the plasmas for the FODO waveform case and the sinusoidal waveform were due to better matched injection, experiments were performed in which the applied voltage waveform was switched from sinusoidal to FODO, or FODO to sinusoidal, only after the plasma was trapped and there could be no more influence on the plasma from the ion source. When the time of the switch from the sinusoidal waveform to the FODO waveform is varied from early in the injection until late in the dumping, it is clear that there is enhancement in the on-axis trapped plasma signal even after the plasma is trapped. Since the number of trapped ions does not increase after the plasma is trapped, an increase in the on-axis trapped plasma signal corresponds to a transverse compression of the plasma.

In these experiments, the plasma is injected until t=1.7 ms, and then trapped. The plasma is held for a typical trapping time of 100 ms until t=101.7 ms to simulate long-distance beam propagation over several thousand lattice periods, and is then dumped. Figure 11(a) shows the measured on-axis signal as a function of the time when the applied voltage waveform was changed from FODO to sinusoidal. Except for times after 101.7 ms, when the some of the plasma is already collected on the diagnostic and therefore cannot be influenced by the change in waveform, the data show that changing from FODO to a sinusoidal waveform is equivalent to having applied a sinusoidal waveform for all time. The results shown in Fig. 11(b) demonstrate that, while changing from a sinusoidal waveform to a FODO during injection ($t<1.7$ ms) gives the largest on-axis signal, the signal is still larger than in the pure sinusoidal waveform case even when the change from sinusoidal to FODO occurs during the trapping time (1.7 ms$<t<$101.7 ms). At times greater than 101.7 ms, a portion of the plasma has been collected and cannot be influenced by the change from sinusoidal to FODO. Thus, the improved plasma conditions associated with the FODO waveform cannot be due solely to better matching during injection.

VII. CONCLUSIONS

Controlling emittance growth and limiting halo particle production are important requirements for beam transport systems and these phenomena can occur as the result of many varied causes. Using the PTSX to study the transport of intense charged-particle beams in a compact laboratory experiment, emittance growth and halo particle production have been studied in a broad range of experiments. Random noise-induced emittance growth and halo particle production have been investigated both in experiments with white noise and with colored noise when accompanied by beam mismatch oscillations. Changes in the average transverse focusing frequency ω_q can be implemented to compress the beam, but must be applied adiabatically in order to avoid emittance growth and halo particle production. Finally, using a FODO waveform instead of a sinusoidal waveform allows plasmas to be trapped that begin with higher normalized intensities $\hat{s}$ and a lower initial emittance. In addition to more accurately simulating the magnetic field structure in beam transport systems, the high $\hat{s}$, low emittance plasmas will provide a useful baseline for future experiments exploring intense beam phenomena.

ACKNOWLEDGMENTS

This research was supported by the U.S. Department of Energy.

[1]R. C. Davidson and H. Qin, *Physics of Intense Charged Particle Beams in High Intensity Accelerators* (World Scientific, Singapore, 2001).
[2]M. Reiser, *Theory and Design of Charged Particle Beams* (Wiley, New York, 1994).
[3]A. W. Chao, *Physics of Collective Beam Instabilities in High Energy Accelerators* (Wiley, New York, 1993).
[4]See, for example, Proceedings of the 2003 Particle Accelerator Conference, pp. 1–3571.
[5]P. G. O'Shea, M. Reiser, R. A. Kishek, S. Bernal, H. Li, M. Pruessner, V. Yun, Y. Cui, W. Zhang, Y. Zou, T. Godlove, D. Kehne, P. Haldemann, and I. Haber, Nucl. Instrum. Methods Phys. Res. A **464**, 646 (2001).
[6]N. Kjærgaard and M. Drewsen, Phys. Plasmas **8**, 1371 (2001).
[7]See, for example, Proceedings of the 2004 International Heavy Ion Fusion Symposium, pp. 1–551; Nucl. Instrum. Methods Phys. Res. A **544**, 1 (2005).
[8]W. Paul and H. Steinwedel, Z. Naturforsch. A **8**, 448 (1953).
[9]E. P. Gilson, R. C. Davidson, P. C. Efthimion, and R. Majeski, Phys. Rev. Lett. **92**, 155002 (2004).
[10]S. M. Lund and B. Bukh, Phys. Rev. ST Accel. Beams **7**, 024801 (2004).
[11]L. K. Spentzouris, J.-F. Ostiguy, and P. L. Colestock, Phys. Rev. Lett. **76**, 620 (1996).
[12]D. Neuffer, E. Colton, D. Fitzgerald, T. Hardek, R. Hutson, R. Macek, M. Plum, H. Thiessen, and T.-S. Wang, Nucl. Instrum. Methods Phys. Res. A **321**, 1 (1992).
[13]J. Byrd, A. Chao, S. Heifets, M. Minty, T. O. Raubenheimer, J. Seeman, G. Stupakov, J. Thomson, and F. Zimmerman, Phys. Rev. Lett. **79**, 79 (1997).
[14]R. C. Davidson, H. Qin, and G. Shvets, Phys. Plasmas **7**, 1020 (2000).
[15]H. Okamoto and H. Tanaka, Nucl. Instrum. Methods Phys. Res. A **437**, 178 (1999).
[16]R. Takai, H. Enokizono, K. Ito, Y. Mizuno, K. Okabe, and H. Okamoto, Jpn. J. Appl. Phys., Part 1 **45**, 5332 (2006).
[17]K. Ito, K. Nakayama, S. Ohtsubo, H. Higaki, and H. Okamoto, Jpn. J. Appl. Phys. **47**, 8017 (2008).
[18]M. Chung, E. P. Gilson, R. C. Davidson, P. C. Efthimion, and R. Majeski, Phys. Rev. Lett. **102**, 145003 (2009).
[19]M. Chung, E. P. Gilson, R. C. Davidson, P. C. Efthimion, and R. Majeski, Phys. Rev. ST Accel. Beams **12**, 054203 (2009).
[20]M. Chung, E. P. Gilson, M. Dorf, R. C. Davidson, P. C. Efthimion, and R. Majeski, Phys. Rev. ST Accel. Beams **10**, 064202 (2007).
[21]E. P. Gilson, M. Chung, R. C. Davidson, P. C. Efthimion, and R. Majeski, Phys. Rev. ST Accel. Beams **10**, 124201 (2007).
[22]E. P. Gilson, R. C. Davidson, P. C. Efthimion, R. Majeski, and H. Qin, Laser Part. Beams **21**, 549 (2003).
[23]E. P. Gilson, R. C. Davidson, P. C. Efthimion, R. Majeski, and H. Qin, Proceedings of the 2003 Particle Accelerator Conference, 2003, p. 2655.
[24]E. P. Gilson, M. Chung, R. C. Davidson, P. C. Efthimion, R. Majeski, and E. A. Startsev, Nucl. Instrum. Methods Phys. Res. A **544**, 171 (2005).
[25]M. Chung, E. P. Gilson, M. Dorf, R. C. Davidson, P. C. Efthimion, and R. Majeski, Phys. Rev. ST Accel. Beams **10**, 014202 (2007).
[26]M. Chung, Ph.D. thesis, Princeton University, 2008.
[27]E. P. Gilson, R. C. Davidson, P. C. Efthimion, R. Majeski, and E. A. Startsev, AIP Conf. Proc. **692**, 211 (2003).
[28]C. L. Bohn and I. V. Sideris, Phys. Rev. Lett. **91**, 264801 (2003).
[29]F. Gerigk, Phys. Rev. ST Accel. Beams **7**, 064202 (2004).
[30]J. Qiang, R. D. Ryne, B. Blind, J. H. Billen, T. Bhatia, R. W. Garnett, G. Neuschaefer, and H. Takeda, Nucl. Instrum. Methods Phys. Res. A **457**, 1 (2001).
[31]A. Friedman, D. P. Grote, and I. Haber, Phys. Fluids B **4**, 2203 (1992).
[32]I. V. Sideris and C. L. Bohn, Phys. Rev. ST Accel. Beams **7**, 104202 (2004).
[33]S. Y. Lee, *Accelerator Physics* (World Scientific, Singapore, 2004).
[34]M. Dorf, R. C. Davidson, and E. A. Startsev, Phys. Rev. ST Accel. Beams **9**, 034202 (2006).
[35]E. P. Gilson, M. Chung, R. C. Davidson, M. Dorf, D. Grote, P. C. Efthimion, R. Majeski, and E. A. Startsev, Nucl. Instrum. Methods Phys. Res. A **577**, 117 (2007).